

## Superhydrophobic Properties of Nonaligned Boron Nitride Nanotube Films

Lu Hua Li<sup>†,‡</sup> and Ying Chen<sup>\*†</sup>

<sup>†</sup>Institute for Technology Research and Innovation, Geelong Technology Precinct, Deakin University, Waurn Ponds, Victoria, 3217, Australia and <sup>‡</sup>Department of Electronic Materials Engineering, Research School of Physics and Engineering, the Australian National University, Canberra, ACT, 0200, Australia

Received September 24, 2009. Revised Manuscript Received November 25, 2009

Superhydrophobicity is highly desirable for numerous applications. Here, we report that a semierect but nonaligned boron nitride nanotube (BNNT) film showed superhydrophobicity with contact angle above 170° and a small contact angle hysteresis. This superhydrophobicity was stable over a large range of drop sizes, and the measured critical transition pressure was about 10 kPa. However, the prostrate BNNT films only showed hydrophobicity. The drop retraction behavior during evaporation, the pressure effect on contact angle, the critical transition pressure, the drop impact behavior, and the self-cleaning efficiency between these two kinds of films were systematically investigated and compared.

### 1. Introduction

The lotus has been a sacred symbol in many cultures since ancient times, mainly due to the purity and unattachment it represents. Water drops run easily off their leaves and carry dirt with them. This extreme resistance to wetting, or superhydrophobicity, is usually characterized by a water contact angle larger than 150° and hysteresis smaller than 10°.<sup>1</sup> Less marked antiwetting properties are only termed hydrophobicity. Superhydrophobicity is highly desirable for numerous applications, such as water repellent and self-cleaning coatings,<sup>2</sup> microfluidic lab-on-a-chip systems for chemical, biological, and medical analyses,<sup>3</sup> and low water friction surface for ocean freighters.<sup>4</sup> The contact angle of the lotus leaf can reach 170° due to its cutin and lipid covering as well as its hierarchical micro and nano double structure.<sup>5,6</sup> The latter is crucial for achieving superhydrophobicity, as chemical composition alone can only give hydrophobicity with contact angle less than 120°.<sup>7</sup>

Hexagonal boron nitride (*h*BN) has a layered structure similar to that of graphite, but with boron and nitride atoms arranged alternatively, a melting point near 3000 °C, and high chemical inertness.<sup>8</sup> Another well-known property of *h*BN is its low wettability to molten metals and polymers.<sup>9,10</sup> Because of its excellent lubricity at both low and high temperatures (up to 900 °C),<sup>8</sup> *h*BN powder is widely used as a refractory material in foundry and polymer processing. However, *h*BN is wettable to water.<sup>11</sup> Boron nitride nanotubes (BNNTs) can be viewed as *h*BN sheets rolled up into seamless tubes with nanosized diameter.

They inherit many excellent properties from *h*BN, such as high thermal conductivity and good stability at high temperature.<sup>12–15</sup> BNNTs have a wide bandgap around 6 eV regardless of their chirality, which makes them promising candidates for nano-optoelectronic applications.<sup>16–18</sup> BNNTs also acquire some properties not available from *h*BN, such as high elastic modulus.<sup>19</sup> With their small diameter and high curvature, BNNTs should have better antiwetting properties than *h*BN, due to the positive Laplace pressure that makes liquids on fibers unstable.<sup>20</sup> In addition, with the nanoroughness, superhydrophobicity has already been observed for thin films of BNNTs grown on substrate.<sup>21</sup> Here, we demonstrate that as-grown nonaligned semierect BNNT films produced by a boron (B) ink method can be superhydrophobic with contact angle above 170° and hysteresis of 3.8°. This antiwetting property was stable over a large range of drop sizes, and the critical pressure for transitioning from Cassie state to Wenzel state was estimated to be around 10 kPa. The low fractional contact area ( $f_s$ ) and huge roughness created by the semierect BNNT film were two of the main reasons for achieving superhydrophobicity. If the as-grown BNNTs were prostrate (bent over), only hydrophobicity was observed. The superhydrophobic and hydrophobic BNNT films exhibit distinct drop retraction behaviors during evaporation, drop impact behaviors, and self-cleaning efficiencies. The possible reasons for these differences are discussed. The B ink method enables easy and economic coating of large-area thin films of pure BNNTs on different substrates.

### 2. Experimental Section

**2.1. Synthesis of BNNT Films.** The BNNT films were produced by the following B ink method, which is a new pro-

- \*Corresponding author. E-mail: ian.chen@deakin.edu.au.  
(1) Wang, S.; Jiang, L. *Adv. Mater.* **2007**, *19*, 3423–3424.  
(2) Nakajima, A.; Hashimoto, K.; Watanabe, T.; Takai, K.; Yamauchi, G.; Fujishima, A. *Langmuir* **2000**, *16*, 7044–7047.  
(3) Choong, C.; Milne, W. I.; Teo, K. B. K. *Int. J. Mater. Form.* **2008**, *1*, 117–125.  
(4) Genzer, J.; Efimenko, K. *Biofouling* **2006**, *22*, 339–360.  
(5) Neinhuis, C.; Barthlott, W. *Ann. Botany* **1997**, *79*, 667–677.  
(6) Barthlott, W.; Neinhuis, C. *Planta* **1997**, *202*, 1–8.  
(7) Blossey, R. *Nat. Mater.* **2003**, *2*, 301–306.  
(8) Lipp, A.; Schwetz, K. A.; Hunold, K. *J. Eur. Ceram. Soc.* **1989**, *5*, 3–9.  
(9) Shen, P.; Fujii, H.; Nogi, K. *J. Mater. Sci.* **2007**, *42*, 3564–3568.  
(10) Seth, M.; Hatzikiriakos, S. G.; Clerc, T. M. *Polym. Eng. Sci.* **2002**, *42*, 743–752.  
(11) Rathod, N.; Hatzikiriakos, S. G. *Polym. Eng. Sci.* **2004**, *44*, 1543–1550.  
(12) Chang, C. W.; Han, W. Q.; Zettl, A. *Appl. Phys. Lett.* **2005**, *86*, 173102.  
(13) Chang, C. W.; Fennimore, A. M.; Afanasiev, A.; Okawa, D.; Ikuno, T.; Garcia, H.; Li, D. Y.; Majumdar, A.; Zettl, A. *Phys. Rev. Lett.* **2006**, *97*, 085901.

- (14) Golberg, D.; Bando, Y.; Kurashima, K.; Sato, T. *Scr. Mater.* **2001**, *44*, 1561–1565.  
(15) Chen, Y.; Zou, J.; Campbell, S. J.; Le Caer, G. *Appl. Phys. Lett.* **2004**, *84*, 2430–2432.  
(16) Park, C. H.; Spataru, C. D.; Louie, S. G. *Phys. Rev. Lett.* **2006**, *96*, 126105.  
(17) Chen, H.; Chen, Y.; Liu, Y.; Xu, C. N.; Williams, J. S. *Opt. Mater.* **2007**, *29*, 1295–1298.  
(18) Yu, J.; Yu, D. H.; Chen, Y.; Chen, H.; Lin, M. Y.; Cheng, B. M.; Li, J.; Duan, W. H. *Chem. Phys. Lett.* **2009**, *476*, 240–243.  
(19) Suryavanshi, A. P.; Yu, M. F.; Wen, J. G.; Tang, C. C.; Bando, Y. *Appl. Phys. Lett.* **2004**, *84*, 2527–2529.  
(20) Neimark, A. V. *J. Adhes. Sci. Technol.* **1999**, *13*, 1137–1154.  
(21) Lee, C. H.; Drelich, J.; Yap, Y. K. *Langmuir* **2009**, *25*, 4853–4860.

cess developed from the ball-milling and annealing method.<sup>22</sup> Nanosized B particles were first prepared by ball-milling amorphous B powder (95–97%, Fluka) in ammonia gas ( $\text{NH}_3$ ) at 300 kPa for 150 h. The ball-milled B particles were then dispersed into cobalt nitrate ( $\text{Co}(\text{NO}_3)_2$ ) ethanol solution in an ultrasonic bath for 1 h to form an ink-like solution (B ink). The ink was brushed onto stainless steel substrates with any desired pattern. Finally, the substrate with ink was annealed in nitrogen with 15% hydrogen (15%  $\text{H}_2 + \text{N}_2$ ) reaction gas at 1100 °C from 0.5 to 3 h to form BNNT film.

**2.2. Contact Angle Measurements.** An optical contact angle and surface tension instrument (CAM 101, KSV) was used to measure contact angle, drop volume, and drop contact diameter. Both a flat-headed stainless steel needle (gauge 24) and a glass capillary tube (tip size 60  $\mu\text{m}$ ) were used to dispense deionized water. To measure hysteresis, the drops (~10  $\mu\text{L}$ ) were evaporated in the laboratory environment ( $20 \pm 2^\circ\text{C}$ ,  $65 \pm 2\%$  RH). The contact angles under pressure were obtained by altering the drop volumes from 0.1 to 30  $\mu\text{L}$ . For the critical transition pressure, the films were submerged in deionized water at different depths (10–100 cm) for 1 min and subjected to small vibrations. The pH effect was measured using diluted sulfuric acid ( $\text{H}_2\text{SO}_4$ ) (98%, Merck) and sodium hydroxide (NaOH) pellets (Ajax FineChem) dissolved in deionized water. All contact angle values were average results from 5 to 10 measurements (see Supporting Information).

**2.3. Drop Impact and Self-Cleaning Tests.** The dynamic response of drops falling on the BNNT films was revealed by capturing images at one frame per 33 ms. Water drops with diameter of ~2.1 mm were released from a height of 5 mm (the height of the needle tip). For self-cleaning tests, copper particles (<10  $\mu\text{m}$ , Sigma-Aldrich) were sprayed on the BNNT films. The self-cleaning efficiency was determined by the rolling off of drops with or without initial kinetic energy. Drops without initial kinetic energy were static drops placed on the films and then rolled off by tilting the films at 5–20°. Drops with initial kinetic energy were drops released from 10 mm above films tilted at 40°. The cleaning efficiencies were estimated from both optical microscope and scanning electron microscope (SEM) images.

**2.4. Characterization Techniques.** Zeiss Supra 55 VP and Leo 1530 instruments were used to investigate the surface morphologies of the BNNT films and their cleaning effects. The  $f_s$  values were illustrated by using a SEM image analysis technique in which Photoshop software was used to only retain pixels above the threshold brightness 212 in the SEM images.<sup>21,23</sup> X-ray energy dispersive spectroscopy (EDS) attached to a Hitachi 4300SE/N SEM was used for the examination of the chemical composition of the nanotubes. An Olympus BX51 M optical microscope with a camera (DP12, ColorView) attached was used to acquire particle cleaning images.

### 3. Results and Discussion

**3.1. Superhydrophobic BNNT Films.** BNNT films prepared by the B ink method were firmly adhered to the stainless steel substrate. The films were white and had high purity. Majority of nanotubes showed a bamboo-like structure and relatively smooth exterior surfaces (see Supporting Information, Figure S1). In total, eight BNNT films produced under similar synthesis conditions were tested for their wetting properties. Among these samples, four BNNT films gave relatively high equilibrium contact angles ( $\theta_e$ ),  $171.7 \pm 4.2^\circ$ ,  $169.1 \pm 3.8^\circ$ ,  $167.8 \pm 3.6^\circ$ , and  $167.4 \pm 5.9^\circ$ . These are rather high values compared to some of the reported results from as-grown CNT

(22) Chen, Y.; Fitz Gerald, J. D.; Williams, J. S.; Bulcock, S. *Chem. Phys. Lett.* **1999**, *299*, 260–264.

(23) Royall, C. P.; Donald, A. M. *Scanning* **2002**, *24*, 305–313.

(24) Li, H. J.; Wang, X. B.; Song, Y. L.; Liu, Y. Q.; Li, Q. S.; Jiang, L.; Zhu, D. B. *Angew. Chem., Int. Ed.* **2001**, *40*, 1743–1746.

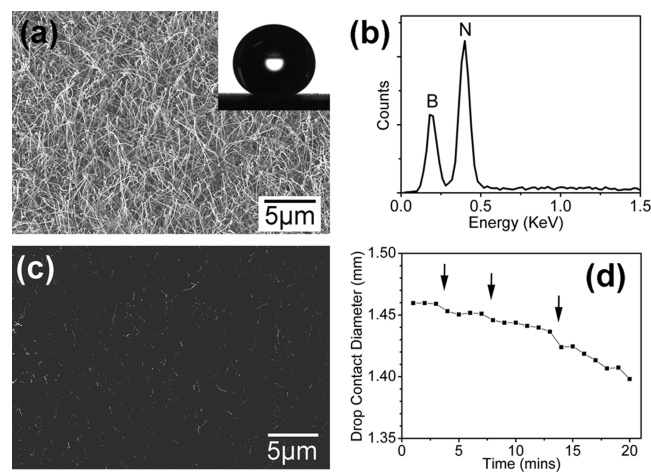


**Figure 1.** (a) SEM image of the semierect BNNT film tilted at 30°; the insert shows an almost round 9.85  $\mu\text{L}$  drop on the film. (b) EDS spectra confirm these are BNNTs. (c) Processed SEM image for estimating the contact area between this BNNT film and drop. (d) Drop contact diameter change during evaporation with the arrows indicating the baseline retraction movements of the drop.

and BNNT films.<sup>21,24–26</sup> Figure 1a shows the SEM image of the BNNT film (30° titled) with  $\theta_e$  larger than 170°. It can be seen that most BNNTs are semierect, i.e., self-standing but tilted or bent, on the substrate. They are not vertically aligned because of the lack of mutual support due to the relatively low nanotube density. These BNNTs are 2–6  $\mu\text{m}$  long. The inset in Figure 1a is a typical image of a drop (9.85  $\mu\text{L}$ ) sitting on this film. EDS confirmed the expected chemical composition of the nanotubes (Figure 1b).

The contact angle hysteresis of the film was measured by the evaporation method for better accuracy (see Supporting Information),<sup>27</sup> and the sessile drop method was also used for comparison. The change in drop contact diameter with evaporation time for this semierect BNNT film is shown in Figure 1d (starting drop volume 9.40  $\mu\text{L}$ ). The sudden retractions of the contact diameter can be clearly seen, for example, from 3 to 4 min and from 7 to 8 min (indicated by arrows). After every retraction, the initial contact angle ( $\theta_o$ ) should be smaller than  $\theta_a$ , but a little bigger than  $\theta_e$  (in fact, the difference between  $\theta_a$  and  $\theta_e$  for this film is very small,  $1.52 \pm 0.68^\circ$ , determined by the glass capillary tube). Here, we assume that  $\theta_o \approx \theta_e$ . Since the value of  $\theta_r$  is related to the size of the drop,<sup>27,28</sup> we turned to the differences between the contact angles after one retraction and before the next, that is,  $\theta_o - \theta_r$ . Therefore, the hysteresis can be calculated from the sum  $(\theta_a - \theta_e) + (\theta_o - \theta_r)$ , which is  $3.8^\circ$  for this film (2.7° by the sessile drop method). The other three films showed similar hysteresis values. So, these four BNNT films are superhydrophobic.

The large contact angle and small hysteresis suggest a Cassie state, in which the drop sits partly on BNNTs and partly on air. The Cassie–Baxter equation can be applied:<sup>29,30</sup>

$$\cos \theta^* = f_s \cos \theta - (1 - f_s) \quad (1)$$

(25) Lau, K. K. S.; Bico, J.; Teo, K. B. K.; Chhowalla, M.; Amaralunga, G. A. J.; Milne, W. I.; McKinley, G. H.; Gleason, K. K. *Nano Lett.* **2003**, *3*, 1701–1705.

(26) Zhu, L. B.; Xu, J. W.; Xiu, Y. H.; Sun, Y. Y.; Hess, D. W.; Wong, C. P. *J. Phys. Chem. B* **2006**, *110*, 15945–15950.

(27) Erbil, H. Y.; McHale, G.; Rowan, S. M.; Newton, M. I. *Langmuir* **1999**, *15*, 7378–7385.

(28) Lafuma, A.; Quere, D. *Nat. Mater.* **2003**, *2*, 457–460.

(29) Cassie, A. B. D.; Baxter, S. *Trans. Faraday Soc.* **1944**, *40*, 546–550.

(30) Bico, J.; Marzolin, C.; Quere, D. *Europhys. Lett.* **1999**, *47*, 220–226.

where  $\theta^*$  represents the contact angle of a drop on a composite surface with solid and air;  $f_s$  is the fractional area of a drop sitting on solid; and  $\theta$  is Young's contact angle on a perfectly flat solid surface. Here, the Young's contact angle of flat BNNT walls, rather than hBN, should be used, because the wetting property of nanotube could differ enormously from that of bulk material.  $\theta$  on flat BNNT walls can be calculated from Young's equation<sup>26</sup>

$$\cos \theta = \frac{\gamma_{SV} - \gamma_{SL}}{\gamma_{LV}} \quad (2)$$

where  $\gamma_{SV}$ ,  $\gamma_{SL}$ , and  $\gamma_{LV}$  are the solid/vapor, solid/liquid, and liquid/vapor surface tensions. The surface tension of a BNNT with diameter about 40 nm has been reported previously, 26.7 mN/m, and the surface tension between water and an individual BNNT was 25.8 mN/m or theoretically 21.1 mN/m.<sup>31</sup> Though our BNNTs have larger diameters (40–80 nm), from a theoretical point of view, this should not have a big influence on these values.<sup>20,31</sup> Therefore,  $\theta$  for BNNTs can be deduced to be 85.6–89.3°. This value is much larger than the Young's contact angles of pressed pellets of hBN particles and of directly grown hBN films,<sup>11,21</sup> but comparable to that of CNTs.<sup>26,32</sup> This value arises because the positive Laplace pressure introduced by the very small nanotube diameter opposes the disjoining pressure and prevents spreading of a water film on the tube surface.<sup>20,31</sup> Then, based on eq 1,  $f_s$  is calculated to be 0.0097–0.0103. In addition,  $f_s$  may be qualitatively illustrated from the processed SEM image by counting the percentage of pixels above a preset brightness threshold. A processed SEM image (nontilted) of this film (Figure 1c) clearly shows that predominantly the tips of the semierect BNNTs have contact with the drop, which leaves most of the drop sitting on air. However, water did not seep or penetrate into the film, even during the lengthy drop evaporation measurement.

**3.2. Hydrophobic BNNT Films.** The other four BNNT films have relatively smaller  $\theta_c$ ,  $159.5 \pm 2.7^\circ$ ,  $158.6 \pm 3.5^\circ$ ,  $155.7 \pm 7.2^\circ$ , and the lowest  $149.0 \pm 2.7^\circ$ . Microscopic investigations found that these films had different BNNT arrangements. The SEM image of Figure 2a shows the surface of the BNNT film (tilted 30°) with  $\theta_c = 159.5^\circ$ , and the insert is a typical image of a drop ( $10.05 \mu\text{L}$ ) on its surface. Unlike the randomly tilted semierect BNNTs in the superhydrophobic films (Figure 1a), BNNTs in these films are prostrate. The BNNTs are lying down because the BNNTs in these films are much longer (15–50 μm) so that their stiffness cannot sustain their own weight (Figure 2a). The processed SEM image (also treated by the same SEM image analysis technique) of this film (Figure 2b) reveals that the drop is sitting on the prostrate BNNT walls instead of their tips, which gives rise to a larger  $f_s$ . From eq 1,  $f_s$  for this film is 0.0588–0.0626, which is about six times that of the semierect film with  $\theta_c$  above  $170^\circ$  (Figure 1a).

Figure 2c shows the change in drop contact diameter with evaporation time (starting drop volume  $10.98 \mu\text{L}$ ). One intriguing observation is that the contact diameter for this film increased slightly at first (until 18 min) and then decreased (from 19 min) during evaporation. This was different from the continually decreasing drop contact diameter observed for the semierect BNNT film (Figure 1d). This observation appears unusual, but was observed to some degree on all the prostrate BNNT films. The most likely explanation is that the drop was slowly spreading

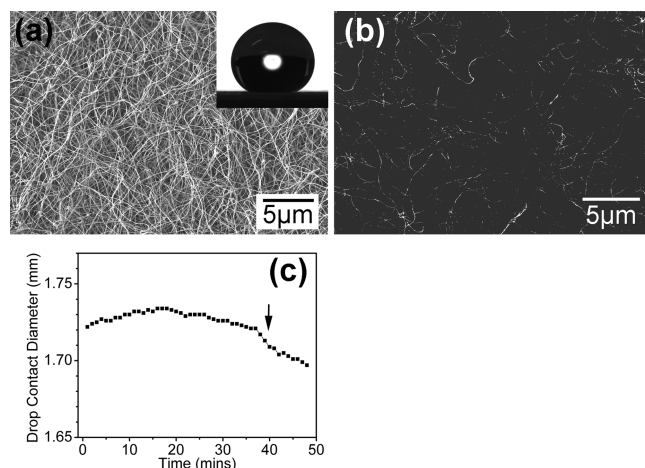


**Figure 2.** (a) SEM image of the prostrate BNNT film tilted at 30°, the insert shows a  $10.05 \mu\text{L}$  drop on the film. (b) Processed SEM image suggesting a larger contact area between BNNTs and drop on this film. (c) Drop contact diameter change during evaporation with the arrow indicating the baseline retraction movement of the drop.

on the prostrate BNNTs without seeping. This phenomenon can be described by the transition from the initial contact angle to the equilibrium contact angle on individual BNNTs. The initial contact angle on a single BNNT ( $\theta_i$ ) is the instant contact angle when the liquid just contacts the BNNT without spreading. If this initial state is not thermodynamically favored, water will spread to form a saturated state, the equilibrium contact angle. In fact, the contact angle of a single BNNT measured by the Wilhelmy method was an equilibrium value.<sup>31</sup> The initial contact angle on a fiber-like material can be estimated by<sup>20</sup>

$$\cos \theta_i = 1 + \frac{1}{\gamma(a + d_0)} \int_{d_0}^{\infty} (a + h) \Pi(h) dh \quad (3)$$

where  $\gamma$  represents the surface tension of water,  $a$  is the radius of fiber or nanotube (average of  $\sim 30$  nm for our BNNTs in the film),  $d_0$  is the Born repulsion length  $\sim 0.158$  nm, and  $\Pi(h)$  is the disjoining pressure. For practical calculations<sup>33</sup>

$$\Pi(h) = \frac{2d_0^2 S_d}{h^3} + \frac{S_p}{l_0} \exp\left(\frac{d_0 - h}{l_0}\right) \quad (4)$$

where  $h$  is the liquid film thickness on solid fiber,  $l_0$  is the correlation length of  $\sim 0.6$  nm,  $S_d$  and  $S_p$  are the apolar and polar components of the initial spreading coefficient ( $S_i$ ).<sup>34</sup>  $S_d$  can be calculated from  $S_d = \gamma_S^d - \gamma_{SL}^d - \gamma_L^d$ , in which  $\gamma_S^d$ ,  $\gamma_{SL}^d$ ,  $\gamma_L^d$  are the apolar components of the surface tensions of BNNTs, between BNNT and water, and of water.  $\gamma_S^d = 22.5$  mN/m,  $\gamma_L^d = 21.8$  mN/m, and  $\gamma_{SL}^d = 0.0055$  mN/m calculated from  $(\gamma_S^d)^{1/2} - (\gamma_L^d)^{1/2}$ .<sup>21,35</sup> So,  $S_d$  is 0.7 mN/m. Then,  $S_p = S_i - S_d = -72.6$  mN/m. Consequently,  $\theta_i$  for water on an individual BNNT is  $90.9^\circ$ . It means that, when a dry BNNT has contact with a drop, water spontaneously spreads on its wall until the equilibrium contact angle reaches  $85^\circ$ . This explains why the observed contact diameter increases on the prostrate BNNT film during evaporation. However, as was observed, this spreading process was very slow and

(33) Thiele, U.; Mertig, M.; Pompe, W. *Phys. Rev. Lett.* **1998**, *80*, 2869–2872.

(34) Shaw, D. J. *Introduction to Colloid and Surface Chemistry*, 4th ed.; Butterworth-Heinemann: Oxford, 1992; Chapter 6.

(35) Van Oss, C. J. *Interfacial forces in aqueous media*, 2nd ed.; CRC Press: New York, 2006; Chapter II.

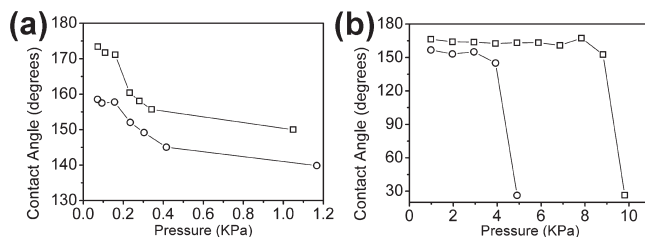


**Figure 3.** (a) Contact angles of the semierect (square) and the prostrate (round) BNNT films under various pressures exerted by different-sized drops. (b) Contact angles after the semierect (square) and prostrate (round) BNNT films were submerged in water at different depths to estimate the critical transition pressure.

inconspicuous, probably due to both the small difference between the initial and equilibrium water contact angles on BNNT and the near-to-nonwetting property of BNNT. In spite of the slight spreading, no catastrophic seeping was found on all four of the prostrate films.

The hysteresis values of the prostrate films are much larger. The film shown in Figure 2a has a hysteresis of  $17.1^\circ$ , measured by the evaporation method ( $13.1^\circ$  by sessile drop method). Figure 2c shows the change in contact diameter of a drop on this film during evaporation. The drop retraction movements were much slower. In Figure 2c, the retraction happened at 37 min and continued for about 5 min. This is totally different from the quick retractions observed from the semierect film. These differences are mainly due to the larger fractional contact areas and different three phase contact line structures of the prostrate BNNT films.<sup>36</sup> The hysteresis resulted from the film shown in Figure 2a is representative of the four prostrate BNNT films. Therefore, these films can only be regarded as hydrophobic.

For vertically aligned CNTs and Si spikes, the contact angle usually increases with increasing nanotube length or spike height, until a constant contact angle value is reached.<sup>37,38</sup> However, for nonaligned nanotube films, or our BNNT films, the nanotube length could have a negative effect on wettability, because extra length may change the nanotube arrangement, especially for nanotubes with small diameters (easier to lie down). For the B ink method, the length of BNNTs mainly depends on the annealing time, if other synthesis conditions are the same. In order to control the tube length to achieve semierect BNNTs and obtain superhydrophobicity, the annealing time should be no longer than 30 min.

### 3.3. Pressure Effect and Critical Transition Pressure.

Various small pressures could be applied to the BNNT films by modifying the sizes of drops statically sitting on the films (see Supporting Information).<sup>28,39</sup> Figure 3a shows the contact angles of the two kinds of BNNT film (Figures 1a and 2a) using different-sized drops. The contact angles of both films decreased synchronously with increasing pressure. At around 1 kPa,  $\theta_e$  for the semierect and the prostrate BNNT films dropped to  $150.5^\circ$  and  $141.1^\circ$ , respectively. This was because the pressure slightly squeezed water into the cavities between nanotubes and thereby increased  $f_s$ . However, for both films at 1 kPa, the drops were still in, or mostly in, the Cassie regime.

To further increase the pressure in order to estimate the critical transition pressure, the films were submerged in deionized water

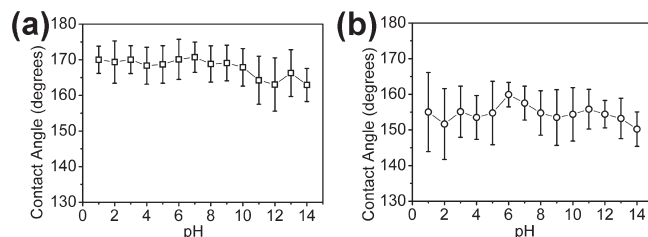


**Figure 4.** Effect of drop pH variations on the contact angle of (a) the semierect BNNT film (square); (b) the prostrate BNNT film (round).

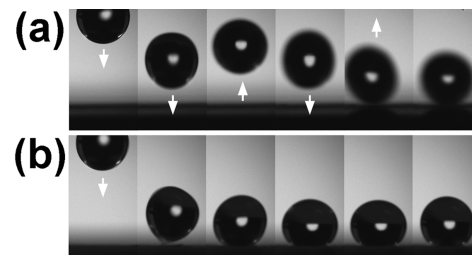


**Figure 5.** Dynamic behavior of a free-falling drop on (a) the semierect BNNT film; (b) the prostrate BNNT film with the arrows indicating the direction of movement of the drop.

at different depths. Figure 3b shows the measured contact angles of the two films immediately after they were removed from the water without drying. These results represent the wettability of each film after the hydrostatic pressure was released or, in other words, the recoverability of their wettability from pressure. Above the critical transition pressure, water could not effectively invade the BNNT films owing to the trapped and compressed air. In this case, the films could totally recover from the hydrostatic pressure and the contact angles of both films, before and after being submerged in water (Figure 3b), were similar. However, once the pressure was too high for the film to sustain, water partly or completely invaded the films and the antiwetting properties were irrecoverably lost and the Wenzel state formed. At about 5 kPa, the prostrate BNNT film was completely wetted with  $\theta_e = 26.3^\circ$ . For the semierect film, the critical transition pressure was about 10 kPa. At about 4 kPa for the prostrate BNNT film and at 8–9 kPa for the semierect film, water was found to partially penetrate a few small areas, but the water invasion at these pressures was still not dramatic enough to completely transit the Cassie states to Wenzel states. These small areas still showed contact angles of  $>110^\circ$ , indicating that the transition into Wenzel states on both BNNT films was not straightforward. Instead, coexistent Cassie and Wenzel states were formed first. The coexistent states were much less stable, because only a little extra hydrostatic pressure could force complete transition. Once the Wenzel state forms, the BNNT films become hydrophilic, because the Young's contact angle of BNNT is slightly below  $90^\circ$  (as shown previously). The main reason for the different critical transition pressures found on the semierect and prostrate films is the different cavity size in the two films. The processed SEM images (Figures 1c and 2b) show that the prostrate BNNT film has larger microcavities than the semierect film because the drop supporting areas for the semierect BNNT film are more evenly arranged. According to the Laplace equation, the liquid invasion pressure is inversely proportional to the pore size, so less pressure is required for water to invade the prostrate BNNT film. The different nanotube arrangement (prostrate or semierect) may also partly contribute to the different critical pressures.

(36) Quere, D. *Nat. Mater.* **2002**, *1*, 14–15.

(37) Fan, J. G.; Dyer, D.; Zhang, G.; Zhao, Y. P. *Nano Lett.* **2004**, *4*, 2133–2138.

(38) Furstner, R.; Barthlott, W.; Neinhuis, C.; Walzel, P. *Langmuir* **2005**, *21*, 956–961.

(39) Yoshimitsu, Z.; Nakajima, A.; Watanabe, T.; Hashimoto, K. *Langmuir* **2002**, *18*, 5818–5822.

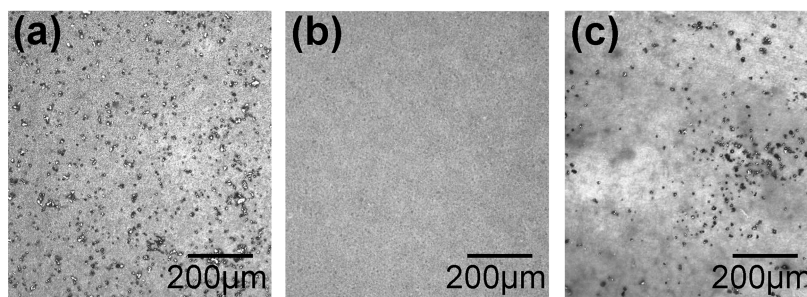


**Figure 6.** (a) Optical microscope image of copper particles smaller than  $10\text{ }\mu\text{m}$  (dark dots) spread on BNNT film for the self-cleaning test. (b) Semierect BNNT film thoroughly cleaned after a static drop rolled off. (c) Still many particles left on the prostrate BNNT film after the same cleaning.

After the invaded water dried, most areas of both films had lost their nonwetting property. SEM investigation showed that the standing BNNTs were flattened and the long BNNTs became entangled and more densely packed (see Supporting Information, Figure S2). These changes enormously reduced the surface roughness of both films so that Cassie states were no longer sustainable.

However, after a Scotch tape was pulled off a prostrate BNNT film (whether the film has been water-invaded or not), the film suddenly became superhydrophobic. For example, by sticking tape onto the water-invaded prostrate film (the film in Figure 2a and Supporting Information Figure S2b) and then mechanically pulling the tape off, the film suddenly had  $\theta_e = 169.3 \pm 4.8^\circ$  and hysteresis of several degrees. This dramatic change was caused by the long nanotubes on the film surface being removed by the tape, and the new surface now had high roughness and low fractional area (see Supporting Information, Figure S3).

**3.4. pH Effect.** Because of the chemical inertness of BNNTs and the small fractional area of the films, even strongly acidic and basic conditions do not affect the antiwetting properties of BNNT films.<sup>21</sup> For the semierect BNNT film,  $\theta_e$  showed little change with variations in the pH of the drop, although a slight decrease in  $\theta_e$  was observed at pH 11–14 (Figure 4a). For the prostrate BNNT film,  $\theta_e$  values were affected slightly more by strongly acidic and basic drops, and the standard deviation of the contact angle results was also larger (Figure 4b). The pH value showed a bigger influence on the prostrate film mainly because it had larger  $f_s$ . The lower critical transition pressure of the prostrate film may also make it less stable and more easily affected by chemicals.

**3.5. Drop Impact.** The drop impacting velocity, calculated from the drop release height, was  $0.23\text{ m/s}$ . The corresponding Weber number ( $We$ ) was 1.6. The drops showed totally different behaviors after impinging the two kinds of film. For the semierect BNNT film (Figure 5a), the drop completely rebounded from the surface several times before, in most cases, bouncing off the film. The estimated restitution coefficient ( $\varepsilon$ ) for the first bounce off this film was 0.79. During the drop impact, kinetic energy was transferred via the liquid surface tension, the contact angle hysteresis, and the drop oscillation.<sup>40</sup> Water may also intrude into the film and dissipate some energy.<sup>41</sup> This possibility can be estimated by calculating the maximum drop impact pressure exerted on the film. If the propagation of compressional waves, viscosity and surface tension are all neglected, and we can estimate<sup>42</sup>

$$P_{\max} = \rho v_{\max}^2 \quad (5)$$

where  $P_{\max}$  is the maximum impact pressure,  $\rho$  is the density of water, and  $v_{\max}$  is the impacting velocity of the water drop. Note that this estimate is too small for rigid solid surfaces, but suitable for nonhomogeneous surfaces.<sup>43</sup> The maximum pressure from the falling drop was about 67 Pa. The likely effect of this pressure can be determined by referring to Figure 3a and b. It can be seen that this pressure was too small to cause penetration of water into the film because of the trapped and compressed air.

For the prostrate BNNT film (Figure 5b), the drop hardly showed any rebound. Instead, it was pinned and then pulsated on the film. The lack of bounce on this film can be partly blamed on its higher hysteresis; yet, it should not be the only reason, because a surface with contact angle  $160^\circ$  and hysteresis  $30^\circ$  can still show bounce with high elasticity.<sup>40</sup> Water intrusion is unlikely to be a major reason either, because (1) the estimated maximum drop pressure is also too small for this film, as the previous calculation showed; (2) the drop kept its round shape and did not show a dramatic increase in the receded angle during the retraction phase (when the drop moved upward); and (3) the contact angle after the drop stabilized on this film showed similar values to those measured by the sessile method. Another possible reason for the lack of bounce may be the deformation of the film surface. For the prostrate film, long BNNTs lie loosely on each other and there are a great number of voids in the film. These voids allow the nanotubes to be compressively strained when the drops impinge on them. However, the same deformation does not appear to occur on the semierect BNNT films.

**3.6. Self-Cleaning Efficiency.** One important application of the superhydrophobic surface is self-cleaning and anticoating.<sup>6,38,44</sup> Irregularly shaped copper particles were homogeneously sprayed on two films for the cleaning tests (Figure 6a). The size of these particles was  $2\text{--}10\text{ }\mu\text{m}$ . The cleaning efficiencies were first tested by tilting the BNNT films with static drops sitting on them (drops without initial kinetic energy). The semierect film showed almost perfect cleaning along the drop rolling-off path: almost fleckless under optical microscope (Figure 6b). SEM revealed only a very small number of particles with sizes  $\sim 2\text{ }\mu\text{m}$  still left on this film (see Supporting Information, Figure S4). The estimated percentage of particles remained was  $<2.5\%$ . In contrast, about 50% of particles remained on the prostrate BNNT film after a similar cleaning process (Figure 6c and also see Supporting Information, Figure S4). It took three to four static drop cleaning passes to remove most of particles from this film. In the test, both films could allow fast rolling-off drops when tilted. However, the copper particles could be trapped and carried in front of the fast rolling-off drop without redepositing only if the

(40) Richard, D.; Quere, D. *Europhys. Lett.* **2000**, *50*, 769–775.

(41) Wang, Z.; Lopez, C.; Hirsa, A.; Koratkar, N. *Appl. Phys. Lett.* **2007**, *91*, 023105.

(42) Nearing, M. A.; Bradford, J. M.; Holtz, R. D. *Soil Sci. Soc. Am. J.* **1986**, *50*, 1532–1536.

(43) Nearing, M. A.; Bradford, J. M.; Holtz, R. D. *Soil Sci. Soc. Am. J.* **1987**, *51*, 1302–1306.

(44) Bhushan, B.; Jung, Y. C.; Koch, K. *Langmuir* **2009**, *25*, 3240–3248.

total adhesion between the particle and the film surface (van der Waals forces) was overcome by the particle–water adhesion.<sup>6</sup> The adhesion between the particle and BNNT film is related to  $f_s$ .<sup>44</sup> Higher  $f_s$  usually means higher particle–film adhesion, which makes cleaning more difficult. So, the different  $f_s$  resulted in distinctly different cleaning efficiencies.

Drops with small initial kinetic energy were also used for cleaning tests. The drops were released from 10 mm height to impinge on a 40° tilted BNNT film (impacting velocity about 0.44 m/s). Even for the prostrate BNNT film, most of the copper particles were successfully removed by just one drop. The drop with higher kinetic energy could introduce higher impact pressure on the film surface and lead to higher adhesion forces between water and particles.

#### 4. Conclusions

A nonaligned semierect BNNT film synthesized by a B ink method showed superhydrophobicity with contact angle above 170° and hysteresis less than 4°. However, longer growing times led to prostrate BNNT films, on which only hydrophobic behavior was observed. Detailed comparisons of the drop retraction behavior during evaporation, the pressure effect on contact angle, the critical transition pressure, the drop impact behavior,

and the self-cleaning efficiency between these two kinds of films, gave insights into their distinct wetting properties. These differences could be satisfactorily explained by the differences in fractional surface area, roughness, and compressibility. These results give guidance not only for the design of BNNT films as antiwetting coatings to water, but may also assist in fabricating films for use in molten polymer processing, as BNNTs are more stable than their counterpart carbon nanotubes at high temperatures.

**Acknowledgment.** Luhua Li thanks Dr. Peter Lamb of Deakin University for reading and discussing the manuscript and Dr. Hua Chen of Australian National University for kindly providing glass capillary tubes with microsized tips. Luhua Li also thanks Mr. Christopher Hurren and Mr. Graeme Keating of Deakin University for the assistance for the contact angle measurement. We are grateful for the ARC Centre of Excellence grant.

**Supporting Information Available:** Detailed experimental information. TEM image of BNNTs. SEM images of the water invaded films, the Scotch tape treated film, and the films cleaned by drops without initial kinetic energy. This material is available free of charge via the Internet at <http://pubs.acs.org>.